Removal of Anions PO_4^{3-} and Methyl Orange Using Fe-Modified Biochar Derived from Rice Straw

Do, Phuong My Thi
Department of Environmental Engineering, College of the Environment and Natural Resources, Can Tho University, Can Tho 900000, VIETNAM

Phan, Thanh Tuyen Thi
College of the Environment and Natural Resources, Can Tho University, Can Tho 900000, VIETNAM

Nguyen, Chiem Huu
Department of Environmental Sciences, College of the Environment and Natural Resources, Can Tho University, Can Tho 900000, VIETNAM

Downes, Nigel K.
College of the Environment and Natural Resources, Can Tho University, Can Tho 900000, VIETNAM

Nguyen, Loc Xuan *+
Department of Environmental Sciences, College of the Environment and Natural Resources, Can Tho University, Can Tho 900000, VIETNAM

ABSTRACT: *A novel magnetic biochar (Fe_3O_4-biochar) using rice straw as the raw material and magnetite (Fe_3O_4 nanoparticles) as the objective magnetic medium was successfully synthesized under high-temperature and oxygen-free conditions. Several techniques and methodologies (SEM/EDX, FT-IR, N_2 adsorption-desorption isotherms, and pHpzc measurements) were used to determine the surface functional groups and physicochemical properties of Fe_3O_4-biochar, which showed that the Fe_3O_4-biochar was successfully synthesized and deposited on the surface of the pristine biochar. The surface area of the Fe_3O_4-biochar was measured as 337.77 m^2/g and 0.227 cm^3/g pore volume. Then the adsorption behavior of phosphate (PO_4^{3-}) and Methyl Orange (MO) from the aqueous solution onto the Fe_3O_4-biochar was investigated. The influence of variables including pH, initial concentration of PO_4^{3-}/MO, adsorbent dosage, and contact time was studied in detail. The optimal adsorption amount of PO_4^{3-} (189.2 mg/g) was obtained with 0.1 Fe_3O_4-biochar g/L, at pH of 2 for 240 min; whereas the optimal adsorption amount of MO (37.31 mg/g) was obtained with 0.03 Fe_3O_4-biochar g/L, at pH of 2 for 240 min. The equilibrium data were fitted to both Langmuir and Freundlich isotherms (R^2>0.92 for PO_4^{3-}, R^2 >0.96 for MO). Besides, the pseudo-second-order exhibited a better fit for the kinetic studies (R^2>0.79 for PO_4^{3-}, R^2>0.88 for MO). This study showed that Fe_3O_4-biochar could be utilized as an efficient, magnetically separable adsorbent for the removal of anions PO43 and MO from the aqueous mediums.*

KEYWORDS: *Adsorption; Fe_3O_4-biochar; Methyl orange; Phosphate; Rice straw.*

***** *To whom correspondence should be addressed.*
+ E-mail: nxloc@ctu.edu.vn
1021-9986/2023/3/821-834 *14/$/6.04*

INTRODUCTION

Nutrients (NO_3^- and PO_4^{3-}) are essential elements for biological life, in which phosphate (PO_4^{3-}) is crucial for the growth of living organisms. However, phosphate is also the main driver of eutrophication of lakes, in which phosphate concentrations below 0.02 mg/L can lead to uncontrolled growth of organisms, especially algae [1]. In general, the world's supply of phosphate is mostly derived from *mineral deposits* as the form of phosphate rocks. Phosphate rocks are the raw material used in the production of various phosphatic fertilizers. In *fertilizers, phosphorus* is present in three *forms:* (1) fully water-soluble orthophosphates (PO_4^{3-}, HPO_4^{2-}, and $H_2PO_4^-$); (2) partly water-soluble polymerized orthophosphates, called *polyphosphates*; and, (3) water-insoluble *mineral* and *organic phosphates* [2]. Most phosphatic fertilizers belong to the water-soluble orthophosphate form, which are fully soluble in water and *readily* taken up by plants. As the world's third-largest delta, the Vietnamese Mekong Delta is one of the most productive agricultural areas. It is contributing to more than half of the country's food production. In modern agricultural practices in the Delta, the water-soluble orthophosphate fertilizers are usually applied in large quantities, leading to a build-up of orthophosphate in the lake or surface water ecosystem. Excessive nutrient inputs, usually nitrogen and phosphate, have been shown to be the main cause of eutrophication over the past 30 years in the Delta [3]. This aging process can result in large fluctuations in the lake water quality and trophic status and in some cases periodic blooms of cyanobacteria, which in turn depletes the dissolved oxygen in water bodies. The hypoxia of the water leads to death of flora and fauna, and *ultimately* leads to eutrophication or "dead zones" in lakes [4].

The presence of synthesized dyes in textile effluents is also another environmental concern in the Delta. The effluents from the textile dyeing industry can easily contain methyl orange (MO), as it is widely used in both dyeing and printing textiles. Methyl orange [(MO) dimethylaminoazobenzenesulfonate] is a common and typical azo anionic dye. This water-soluble organic synthetic dye has very high colorability and presents a bright orange color when dissolved in water. Similar to other synthesized dyes, MO *can hinder light penetration,* causing disturbance *to* photosynthesis, thus affect aquatic life [5]. MO contain aromatic and –N = N– groups in their molecules, which are highly toxic, carcinogenic and teratogenic, and are harmful to the environment and organisms [6]. MO is selected as a simulated pollutant in this study is due to its popularity as a dye and pH indicator.

Different physical, biological and chemical techniques for either PO_4^{3-} or MO removal from water and wastewater have been explored by numerous researchers, including chemical precipitation, ion exchange, electrodialysis/ electrocoagulation, reverse osmosis, adsorption and flotation [7-10]. Among them, adsorption is widely accepted as the cost-effective method. Various adsorbents have been developed to remove PO_4^{3-} or MO from water, such as carbon-based materials [11], polymers [12], minerals and their modified compounds [13,14]. Amongst these, biochar has been widely used and promoted as a potential green adsorbent due to its large surface area, high porosity, stability and favorable physical/chemical surface characteristics [15]. Biochar is defined as a porous carbon material consisting of a variety of surface functional groups generated by biomass pyrolysis in a high temperature and oxygen-depleted environment. The precursor biomass sources used for biochar production are typically agricultural residues and forestry wastes. In the Vietnamese Mekong Delta, rice is the main cultivated. In the 2020/2021 period, production was estimated at 24.9 million metric tons for rough rice *(Oryza sativa L.)* and an estimated rice straw residue of about 24 million metric tons [16]. Such vast quantities, suggest that rice straw offers a promising source to produce biochar.

Recently, it has been found that the synthesis of biochar-based composites or biochar-induced nanoparticles, such as magnetic biochar (or Fe_3O_4-biochar), chemically modified biochar or biochar coated nanoparticles, greatly enhance the adsorption capacity of various contaminants [17]. Among them, biochar induced with iron oxide magnetite particles has attracted a lot of attention for the easy of which it is removed from water post treatment, by applying external magnetic fields [18-20]. In previous studies, magnetic biochar or modified biochar adsorbents were shown to exhibit high removal capacity toward phosphate or MO. For example, Fang *et al.* (2020) achieved high phosphate removal rates from acid-extract of incinerated sewage sludge ash, with 129.79 mg of PO_4^{3-} per g of adsorbent used, as a maximum adsorption capacity onto Mg/Ca modified biochar from peanut shells. The biochar interacted with PO_4^{3-}, HPO_4^{2-}, and $H_2PO_4^-$

mainly through Ca-P and Mg-P precipitation mechanisms [21]. In a ferric oxide hydrate/biochar composite, the adsorbents showed adsorption capacity of 51.75 – 56.15 mg PO_4^{3-} /g in swine manure wastewater, mainly due to the formation of inner-sphere complexes through Fe hydrogen bonding [22]. Wang *et al.* (2021) assembled biochar derived from *Eichhornia Crassipes* stems and Fe_3O_4 nanoparticles (Fe_3O_4@BC) and tested Fe_3O_4@BC for the *adsorption* of MO in water. The results showed that Fe^{2+} concentration/pyrolysis temperature, Fe^{2+} concentration/pyrolysis time all had a significant effect on the adsorption rate of MO by Fe_3O_4@BC. The authors also found that electrostatic interaction and H bond formation are the main mechanisms for Fe_3O_4@BC to adsorb MO [23]. Generally, Fe_3O_4-biochar composites can be synthesized via impregnation-pyrolysis and co-precipitation methods, whereas the magnetic species as Fe^{2+}/Fe^{3+} salt is added before pyrolysis (impregnation-pyrolysis) and after pyrolysis (co-precipitation). Between them, the co-precipitation method is the more widely used method due to its straightforward process.

This study investigates the adsorption of phosphate (PO_4^{3-}) and methyl orange (MO) from aqueous solution by Fe_3O_4-biochar derived from rice straw. The precursor biochar was made by pyrolysis in a furnace at 500°C, at a heating rate of 10°C.min^{-1} for 2h in an oxygen-limited environment, whilst the Fe_3O_4-biochar biochar was produced via the chemical precipitation of Fe^{2+} and Fe^{3+}. Batch adsorption experiments were used to explore the effect of pH, biochar dosage, kinetics, isotherms on the adsorption of PO_4^{3-} and MO by Fe_3O_4-biochar adsorbent. The novelty of this study is centred on the study of the Fe-modified biochar adsorbent in the mitigation of both anions PO_4^{3-} and MO from aqueous solutions, with emphasis on their adsorbent capacity, making comparison amongst them. This study would be able to give more insight into the adsorption of either PO_4^{3-} or MO, to better inform future research.

EXPERIMENTAL SECTION

Chemicals

Phosphate standard solution 0.1 mg/mL PO_4^{3-} (purity >99%) and methyl orange MO (purity >99%) were purchased from Sigma-Aldrich. Ferric chloride ($FeCl_3.6H_2O$), ferrous chloride ($FeCl_2.4H_2O$), hydrochloric acid (HCl), sodium hydroxide (NaOH) were provided by Merck (Germany).

Preparation of Fe_3O_4-biochar

Raw rice straw was collected from the Vietnamese Mekong Delta and underwent several preparational steps for precursor biochar production, including: (1) drying and cutting into small pieces of 2 - 4 mm; (2) forming into cylindrical granules; (3) pyrolyzing in a furnace (Model VMF 165, Yamada Denki, Adachi, Tokyo, Japan) at 500°C, 10°C.min^{-1} of heating rate for 2h in an inert nitrogen atmosphere; (4) crushing, and sieving the cooled biochar to the required grain size (<0.075 mm); (5) washing with 0.1M HCl and distilled water until the pH ~6.0 and 7.0 was obtained; (6) drying at 80°C to constant weight, then sieving and storing in tightly closed glass bottles until use for further magnification.

The co-precipitation method was used to synthesize Fe_3O_4-biochar, following a protocol summarized in *Sun et al.*, (2015). Briefly, Fe-hydroxides (i.e., $Fe(OH)_2$ and $Fe(OH)_3$) were precipitated using $FeCl_3.6H_2O$ and $FeCl_2.4H_2O$ (3:1 ratio), typically when stirred under very alkaline (pH ≈ 10) using 5 M NaOH solution [24]. Subsequently, precursor biochar was thoroughly mixed with the Fe-hydroxides suspension at 80°C on a magnetic stirrer for 1h, followed by centrifugating at 3000 rpm for 10 min. The Fe_3O_4-biochar precipitate was finally oven-dried at 60°C to constant weight.

Characterization of Fe_3O_4-biochar

A scanning electron microscopy (SEM), coupled with an energy dispersive X-ray (EDX) spectroscopy (SEM-EDX Hitachi S-4800, Japan) was used to analyse the surface morphology and elemental composition of the Fe_3O_4-biochar. The functional group on the surface of Fe_3O_4-biochar was analyzed using a Fourier transform infrared spectroscopy (FTIR, FTIR-PerkinElmer Spectrum 10.5.2), recorded at the atmospheric pressure with a resolution of 4 cm^{-1}. The nitrogen adsorption isotherm was measured using Nova Station A (Quantachrome Instruments version 11.0, USA).

The point of zero charge (pH_{pzc}) was determined by the pH drift method [25]. Briefly, $CaCl_2$ solution (0.005 M) was boiled to remove CO_2 and was cooled down to room temperature, then was adjusted pH with 0.1 M NaOH or 0.1 M HCl if necessary. Fe_3O_4-biochar (0.06 g) then was added to 20 mL of the pH-adjusted solution, and the solution was shaken for 24 h. The final pH of the solution

after 24 h was recorded, then the difference between initial and final pH (ΔpH) was plotted against initial pH values.

Batch adsorption experiments

Experiments were conducted by batch mode adsorption technique and carried out at room temperature (25±2°C). The *experiments were* done by taking 10 mL of PO_4^{3-}/MO samples in a 15mL falcon tube, thereafter, the parameters including pH, adsorbent mass, adsorption time, PO_4^{3-}/MO concentrations were adjusted depending on the experimental purposes. The tube was agitated at 120 rpm for 30 min, and the residual Fe_3O_4-biochar adsorbed with either PO_4^{3-} or MO ions was filtered using Whatman No. 6 filter paper. Concentrations of PO_4^{3-} and MO were subsequently estimated using UV-Vis spectroscopy (Shimadzu UV-1900, Japan).

The amount of PO_4^{3-}/MO adsorbed on per weight of Fe_3O_4-biochar at equilibrium, q_e (mg/g), and the removal efficiency of PO_4^{3-}/MO, S (%), were calculated according to Eqs. (1) and (2) [26,27]:

$$q_e = \frac{C_0 - C_e}{m} V \quad (1)$$

$$S = \frac{C_0 - C_e}{C_0} 100 \quad (2)$$

Where: V (L) is the volume of PO_4^{3-}/MO solution; m (g) is the weight of Fe_3O_4-biochar; C_0 and C_e (mg/L) are the initial PO_4^{3-}/MO concentrations and PO_4^{3-}/MO concentrations at equilibrium, respectively.

All the experiments in this study were conducted in triplicates, and only the average values are reported with standard deviation.

RESULTS AND DISCUSSION

Physio-chemical characteristics of Fe_3O_4-biochar

The nitrogen adsorption–desorption curve onto Fe_3O_4-biochar is shown in Fig. 1(A). At a low relative pressure ($P/P_s \leq 0.1$), nitrogen adsorption increases linearly with the increase of relative pressure, mainly due to the filling of micropores. When $P/P_s > 0.4$, an approximately closed hysteresis loop is formed, which is mainly due to the strong adsorption of the mesopore [28]. According to the classification by the International Union of Pure and Applied Chemistry (IUPAC), the isotherm of Fe_3O_4-biochar can be classified as being of type IV shape. Type IV shows limiting adsorption at high P/P_s due to the filling of mesopores by capillary condensation. It indicates the initial stages of multilayer adsorption on the mesopore walls occurred as same as over the open surface but at high P/Ps it is limited by the capillary architect of pores. Type IV isotherm indicates the large uptake of nitrogen at relative pressures between 0.5 and 0.9 P/Ps. According to IUPAC classification, the values lie in the mesopore domain. A sharp inflection at a relative pressure in the range of 0.6-0.8 corresponding to the capillary condensation of N_2 indicates the uniformity of the pores of highly mesoporous material [29]. This adsorption is characterized by hyteresis H2 loop. H2 hysteresis loops are known to signal the presence of pores with narrow mouths (ink-bottle pores) or internal mesopores with little to no direct connectivity to the particle surface [30].

The textural properties such as surface area, average pore size, and pore volume were estimated from well-known calculation methods such as the Brunauer–Emmett–Teller (BET) and the Barrett– Joyner–Halenda (BJH). Fig. 1 (B) shows the pore size distributions of the mesoporous Fe_3O_4-biochar estimated by the BJH method from desorption branches. The results showed that the prepared Fe_3O_4-biochar possessed the mesoporous surface with the pore radii at approximately 25 nm. The specific surface area calculated using the BET equation was 337.77 m^2/g and pore volume was 0.227 cm^3/g. These structural analysis results could account for the higher uptake of either phosphate or MO due to a relatively high surface area and well-developed mesoporous pores. Based on physical properties of Fe_3O_4-biochar, a feasibility test for phosphate and MO removal was conducted, and the detailed experimental results are described in the next section.

The FTIR spectra of the Fe_3O_4-biochar were plotted and presented in Fig. 2. The samples were scanned in the range of 4000 to 400 cm^{-1}. In particular, the presence of closely packed spectra in the region around 405 cm^{-1} and 576 cm^{-1} can be ascribed to the oxides of iron due to the presence of Fe_3O_4 in the biochar [31]. The characteristic strong peaks at 712 cm^{-1} are a strong indication of the stretching vibration of aromatic C–H attributed to the Fe_3O_4-biochar. The broad peak at 1039 cm^{-1} is credited to the presence of the symmetric stretching vibrations of C-O-C peaks. The weak peaks observed in the region 1510 - 1625 cm^{-1} indicate the existence of C=C stretching peaks. The peaks at 3700 - 3100 cm^{-1} attributing to the stretching

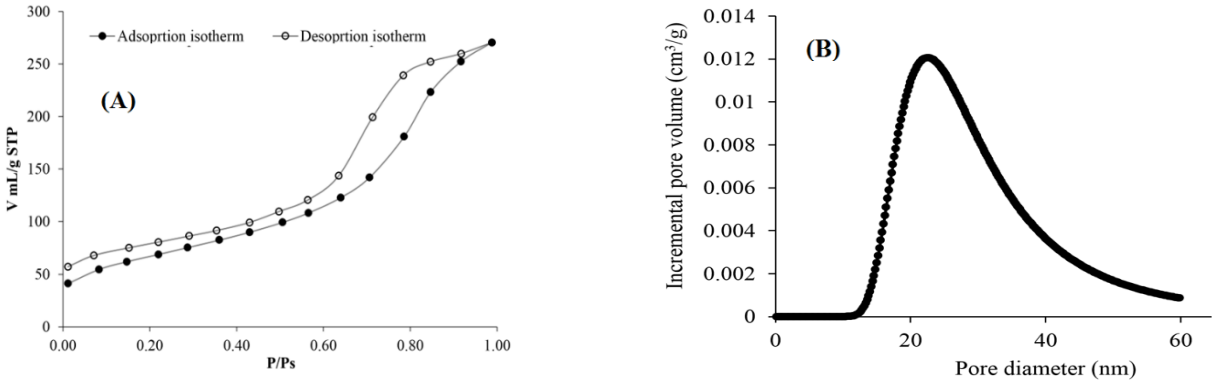

Fig. 1: (A) Adsorption/desorption isotherms of N_2 at 77K; (B) Distribution of pores according to the method BJH.

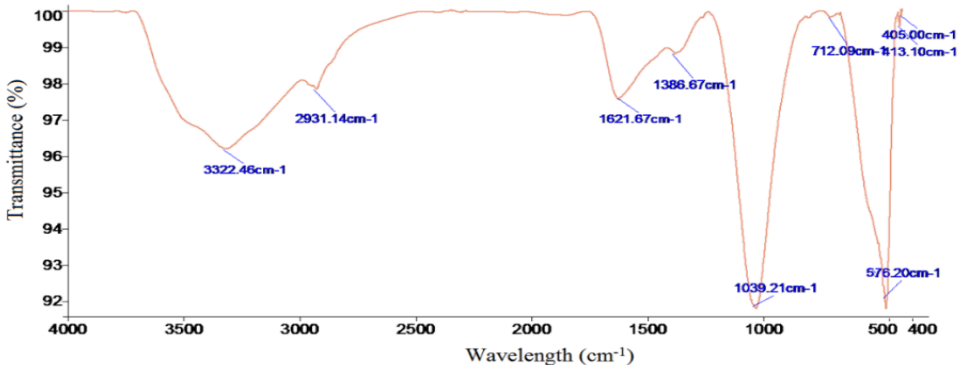

Fig. 2: The FT-IR analysis of Fe_3O_4-biochar.

and bending vibrations of O-H appeared in FT-IR spectra of Fe_3O_4-biochar [32].

The surface morphology and structural properties of the Fe_3O_4-biochar were investigated by SEM and the image is presented in Fig. 3, resembling flake-like structures. The presence of spherical particles on the surfaces of the Fe_3O_4-biochar can be attributed to spherical forms of the spinel-type metal oxides of iron [33]. There is also a pattern of agglomeration of the spherical particles that can be seen in the surfaces of Fe_3O_4-biochar. In summary, the SEM images reveal the morphological and structural properties of the Fe_3O_4-biochar.

EDX analysis shows the presence of the following major elements in the Fe_3O_4-biochar: carbon, oxygen, iron, sodium, silicon, and chloride. The weight compositions of C, O, Fe, Si, Cl, and Na in the Fe_3O_4-biochar were found to be 17.64%, 33.57%, 22.41%, 11.69%, 10.81%, and 3.22%, respectively. The presence of these elements in the Fe_3O_4-biochar supports the FT-IR result.

Adsorption Experiment Results

Effects of pH

Among operating parameters explored, pH is an important parameter that affects the adsorption performance of pollutants in water. This is because pH is widely acknowledged to significantly influences the surface charge of adsorbents [34]. To gain further insights into the effect of pH on phosphate and MO adsorption, values of the point of zero charge (pH_{pzc}) for Fe_3O_4-biochar were computed and presented in Fig. 4 (A). The result shows that Fe_3O_4-biochar had pH_{zpc} of 7.69, indicating that Fe_3O_4-biochar is predominantly positive at pH below 7.69 and thus attracts negatively charged ions (i.e., anions) such as phosphate or methyl orange. Therefore, the Fe_3O_4-biochar surface will favor the adsorption of PO_4^{3-} and MO at pH values lower than pH_{pzc}.

As for the phosphate, the PO_4^{3-}adsorption decreased sharply from 45.92 mg/g to less than 5 mg/g when the initial pH increased from 2 to 10 (Fig. 4 (B)). Under the

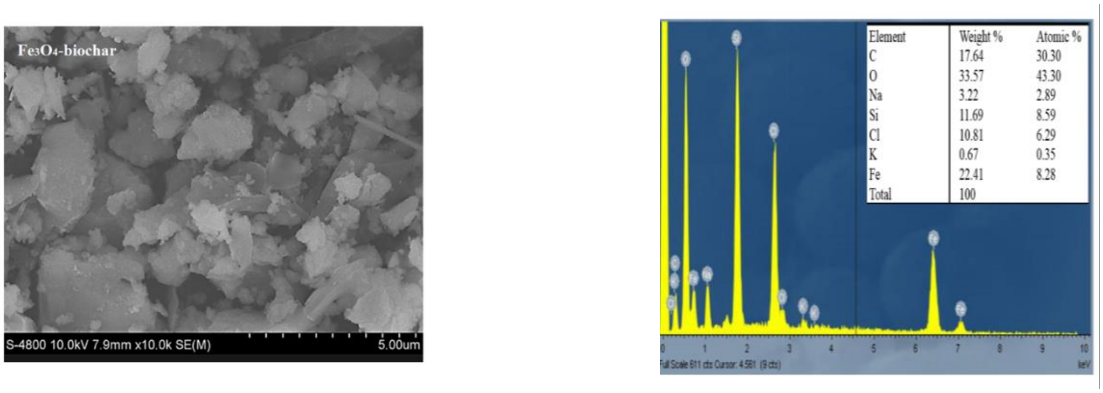

Fig. 3: SEM-EDX analysis of Fe_3O_4-biochar.

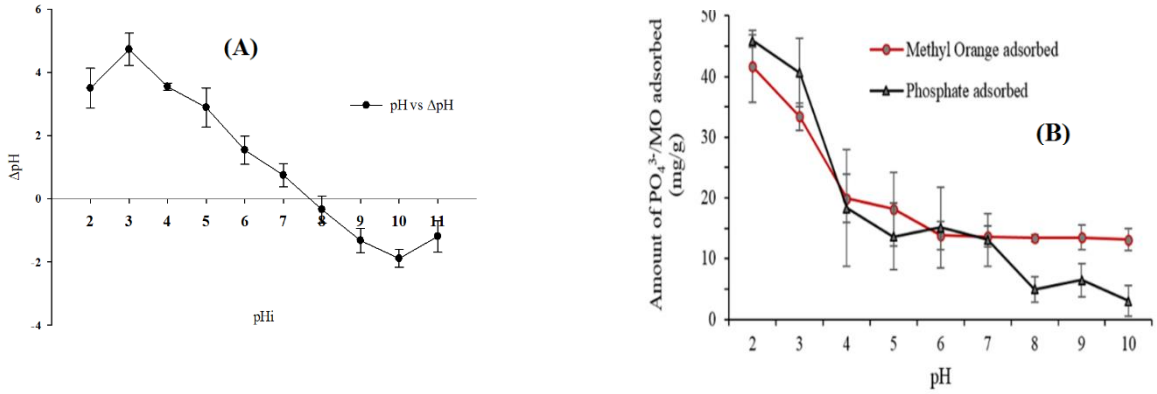

Fig. 4: (A) pHpzc của Fe_3O_4-biochar; (B) The effect of pH on adsorption of PO_4^{3-}/MO.

experimental conditions, phosphate predominantly existed in the anionic forms of monovalent phosphate ion ($H_2PO_4^-$), divalent phosphate ion (HPO_4^{2-}) and phosphate tri-anion (PO_4^{3-}) over the pH range of 2 to 10. The main phosphate anions formed were $H_2PO_4^-$ and HPO_4^{2-} in the pH ranges of 3–7 and 7–9, respectively. At low pH of 2, phosphates will mostly exist as H_3PO_4 [35]. Meanwhile, the surfaces of the Fe_3O_4-biochar (pH_{pzc} = 7.69) were protonated and carried positive charges at low pH. As a result, the positively charged surface of the Fe_3O_4-biochar were more likely to adsorb the negatively charged phosphate anions (HPO_4^{2-} and $H_2PO_4^-$). The higher adsorption capacity of phosphate at lower pH values was attributed to the stronger electrostatic attraction [35]. Conversely, at high initial pH (7-10), the hydroxide ion (OH^-) concentration increases, caused the surfaces of the Fe_3O_4-biochar to hold more negative charges, which would strongly repulse the main phosphate species (HPO_4^{2-} and PO_4^{3-}) in the pH range of 8–10. These negatively charged ions may expected to have competitive effect with these phosphate species for available active sorption sites on the Fe_3O_4-biochar surfaces. Due to the strong electrostatic repulsion between these ions, the amount of the main phosphate ions that are attracted to the Fe_3O_4-biochar reduces, thus resulting in low adsorption capacity of phosphates as shown in Fig. 4 (B). Accordingly, the lower adsorption amount in weak alkaline and alkaline solutions was accounted for in terms of the increased repulsion [35]. On the other hand, some iron in the Fe_3O_4-biochar was easily dissolved and existed as Fe^{3+} at low pH values. Therefore, the chemical precipitation of the Fe^{3+} and P ions as $FePO_4$ may also be have contributed significantly to the phosphate removal [36,37]. The effect of initial pH for the removal of phosphate in magnetic biochar-steel dust composite contining 1.5 g of steel dust indicates an almost similar pattern, demonstrated the best performance at pH of 2 (90 mg/g phosphate), and further increase pH to 12, adsorption capacities of phosphate by the composite adsorbent decreased to 58 mg/g [27].

As for the MO, the MO adsorption capacity by the Fe_3O_4-biochar decreased gradually from 41.63 mg to 14.1 mg/g when the initial pH increased from 2 to 6, but it remains almost stable when then initial pH was increased from 6 to 10 (Fig. 4 (B)). Similar to phosphate adsorption, the adsorption of MO dye molecules is also pH dependent. In aqueous solution around and above pH 7, the MO molecule exists as an anion due to the dissociation of the Na^+ ion. Under acidic conditions, the formation of amphoteric methyl orange molecules occurred due to the H^+ ion attached to the nitrogen atom of azo group [38]. In aqueous solution pH below 3, the MO dye changes from orange to pink colour, indicating that pH influences the ionisation of methyl orange [39]. Fig 4 (B) shows that the adsorption capacity of Fe_3O_4-biochar toward MO favors at pH 2-6 (the pH values of lower than pH_{pzc}). To explain, certain functional groups on the Fe_3O_4-biochar surface were protonated at pH less than 7.69, therefore, electrostatic interaction between MO ions and positively charged Fe_3O_4-biochar surface was favored. The decrease in MO adsorption at higher pH may also be due to the competition between MO and OH^- ions for active sites present on the surface of the Fe_3O_4-biochar in aqueous medium. Similar results were also reported during the MO adsorption by other magnetic biochar adsorbents [26,40].

Briefly, Fe_3O_4-biochar reached its maximum adsorption at pH ~2 with 45.92 mg PO_4^{3-}/g and 41.63 mg MO/g, thus a pH of 2.0 was selected for further experiments.

Effects of adsorbent dosage

Besides pH solution, the adsorbent dosage plays an important role for adsorption process because it determined the capacity of adsorbent for a given initial concentration of phosphate or MO solution. In typical, increasing the dosage to a specific level provides a larger surface area and a greater number of active sites, thereby provides greater opportunity for PO_4^{3-} and MO to be adsorbed on the surface of Fe_3O_4-biochar. Further rise in the dosage, however, results in a constant or marginally decreases in removal efficiency of PO_4^{3-} and MO due to the possible agglomeration of Fe_3O_4-biochar particles. In other words, beyond the optimum dosage level, there is less number of availability active sites leading to less adsorbate-adsorbent interaction and more adsorbent-adsorbent interaction [41]. Therefore, it is necessary to explore the optimal dosage of Fe_3O_4-biochar for PO_4^{3-} and MO. The effect of Fe_3O_4-biochar dosage on adsorption capacity and removal efficiency of PO_4^{3-}/MO was presented in Fig. 5.

In Fig. 5, as dosage of Fe_3O_4-biochar varied from 0.01 to 0.2g, removal percentage of PO_4^{3-} and MO generally increased, with PO_4^{3-} increased from 17 to 94% and MO increased from 36 to 66%; whereas amount of PO_4^{3-} to be adsorbed to Fe_3O_4-biochar gradually decreased from 54.2 to 20.4 mg/g, and MO to be adsorbed to Fe_3O_4-biochar also decreased from 55.6 to 17.3 mg/g. It was found that at 0.1 g Fe_3O_4-biochar, the amount PO_4^{3-} adsorbed by Fe_3O_4-biochar was 32.3 mg/g and more than 92% *removal efficiency* was *reached*. Meanwhile, the optimum value for MO was 29.9 mg/g, with 59.7% removal efficiency was obtained at 0.03 g Fe_3O_4-biochar. Further rise beyond these dosage values did not change their removal efficiency obviously due to a smaller number of availability active sites for adsorption, as mentioned previously. Chaukura et al. (2017) reported a similar trend for the adsorption of MO onto ferric oxide–biochar derived from pulp and paper sludge. Increasing the adsorbent mass from 2.5 up to 12.5 g/L was accompanied by an increase in the percentage removal of MO and achieved 100 % removal of MO at 5 g/L adsorbent dosage [26]. With magnetic biochar-steel dust composites, the effect of adsorbent dosage on the adsorption capacity of phosphate also shows similar adsorption capacity trends. The adsorption capacity of phosphate decreases as the adsorbent dosage is increased from 2 – 20 mg. The maximum adsorption capacity for magnetic biochar-steel dust composites were found to be 153 mg/g and 124 mg/g, respectively, at an adsorbent dosage of 2 mg [27].

Adsorption kinetic analysis

For the batch experiment, the adsorption time and the initial concentration of adsorbents are important factors in determining the adsorption capacity value (q_e, mg/g). In this study, the adsorption capacity of Fe_3O_4-biochar was studied with different contact time (varying from 1 to 720 min), initial PO_4^{3-}/MO concentration of 50 mg/L at room temperature (25±2°C). Here, the adsorption capacity toward both PO_4^{3-} and MO ions tends to increase simultaneously with an increasing contact time (see Fig. 6). A longer contact time presumably, the longer time for PO_4^{3-}/MO ions to interact with the surface of Fe_3O_4-biochar.

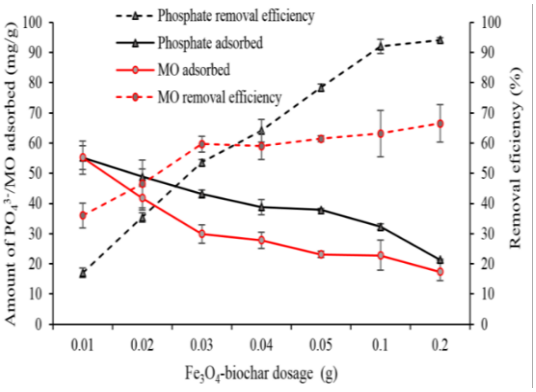

Fig. 5: Effect of Fe_3O_4-biochar dosage on adsorption capacity and removal efficiency of PO_4^{3-}/MO.

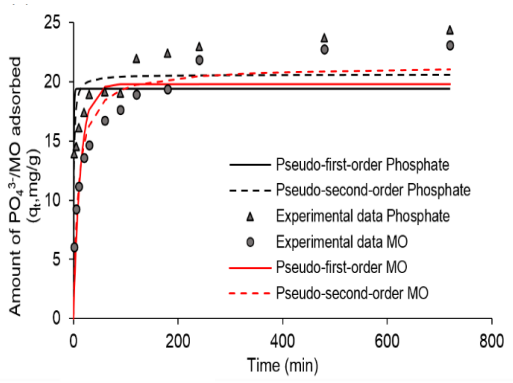

Fig. 6: Non-linear regression pseudo-first-order and pseudo-second-order models for PO_4^{3-}/MO adsorbed onto Fe_3O_4-biochar.

The adsorption values increased significantly in the first 60 min, with the values reaching equilibrium within 240 min. This is probably due to the Fe_3O_4-biochar surface being fully covered with PO_4^{3-}/MO ions after 240 min of contact time.

To examine the adsorption mechanism, pseudo-first-order and pseudo-second-order kinetic models were used to analyze the experimental data. The pseudo–first-order model is based on the assumption that the rate of change of solute uptake with time is directly proportional to difference in saturation concentration and the amount of solid uptake with time, which is generally applicable over the initial stage of an adsorption process. The pseudo–first-order model can be described by the following nonlinear form [41]:

$$q_t = q_e\left(1-\exp^{-k_1 t}\right) \quad (3)$$

where q_e (mg/g) represents the equilibrium adsorption capacity; q_t (mg/g) represents the t time adsorption capacity; k_1 (1/min) represents constant rate of pseudo-first-order adsorption.

The pseudo-second-order model describes the adsorption reaction rate with dependent energetically heterogeneous sites on the adsorbent; it is considered a chemisorptions model. The pseudo-second order model assumed that the rate-determining step might be a chemical sorption involving valence forces through sharing or exchange of electrons between adsorbent and adsorbate. The pseudo–second-order model can be described by the following nonlinear form [41]:

$$\frac{dq_t}{dt} = k_2\left(q_e - q_t\right)^2 \quad (4)$$

where k_2 (g/mg.min) represents constant rate of pseudo-second-order adsorption.

The experimental data of Fe_3O_4-biochar toward PO_4^{3-}/MO fitted with the two kinetic models are shown in the Fig. 6. From their equations, the kinetic constants for PO_4^{3-}/MO adsorption onto Fe_3O_4-biochar are calculated and displayed in Table 1.

It is obviously that the correlation coefficients R^2 value of the pseudo-first-order kinetic equation (0.67 for PO_4^{3-}, 0.75 for MO), was lower than the values obtained by the pseudo-second-order kinetic equation (0.89 for PO_4^{3-}, 0.88 for MO). In addition, the experimental adsorption values ($q_{e,exp}$) of both PO_4^{3-} and MO from the pseudo-second-order kinetic show better fit with their calculated values of the equilibrium adsorption capacity ($q_{e,cal}$). The fit for the pseudo-second-order indicates that the phosphate and MO adsorption on the Fe_3O_4-biochar was conducted through the inner sphere complex. In addition, the chemical sorption mechanism might be the rate controlling step involved in the adsorption process for both PO_4^{3-} and MO ions in the solution [1]. The phosphate or MO adsorption kinetic data fitted to the pseudo-second-order kinetic model were also reported by other Fe-based and metal-containing sorbents [1,26,27]. The formation of chemical bonds is the main factor affecting the pseudo-second-order kinetics of phosphate or MO adsorption in these papers.

Table 1: Kinetic constants for the pseudo-first-order and pseudo-second-order kinetic model.

Adsorbate	Pseudo-first-order				Pseudo-second-order			
	$q_{e,exp}$	$q_{e,cal}$	k_1	R^2	$q_{e,exp}$	$q_{e,cal}$	k_2	R^2
	mg/g	mg/g	1/min		mg/g	mg/g	g/mg.min	
PO_4^{3-}	48.53	31.50	0.00105	0.67	48.53	46.32	0.08476	0.89
MO	23.11	19.82	0.07	0.75	23.11	21.30	0.01	0.88

Adsorption isotherm analysis

For solid–liquid system, the equilibrium of adsorption was one of the important physico-chemical aspects in the description of adsorption behavior. To predict the maximum amount of PO_4^{3-}/MO adsorbed by a unit mass of Fe_3O_4-biochar under equilibrium condition at constant temperature, the Langmuir and Freundlich isotherms were used. The parameters obtained from the two different models provided important information on the sorption mechanisms and the surface properties and affinities of the Fe_3O_4-biochar.

The Langmuir isotherm theory assumes monolayer coverage of adsorbate over a homogeneous adsorbent surface. The nonlinearized Langmuir isotherm equation is represented by Equation below [41]:

$$q_e = \frac{q_m K_L C_e}{1 + K_L C_e} \quad (5)$$

where q_e (mg/g) represents the equilibrium adsorption capacity; q_m (mg/g) represents theoretical maximum adsorption capacity; C_e (mg/L) represents equilibrium concentration of the adsorbate; K_L (L/mg) represents the Langmuir adsorption constant.

The Freundlich isotherm is an empirical equation based on sorption on a heterogeneous surface or surface supporting sites of varied affinities. The nonlinear form of the Freundlich isotherm is given by the following equation [41]:

$$q_e = K_F C_e^{1/n} \quad (6)$$

where K_F ((mg/kg)/(mg/L)^n) represents the sorption affinity; 1/n represents the nonlinearity index (unitless).

Fig. 7 shows the fitting result of Langmuir and Freundlich models. The isotherm parameters obtained from the adsorption experiments are tabulated in Table 2. By comparing the constants and correlation coefficients R^2 (Table 1), it could be seen that for the adsorption of both PO_4^{3-} and MO, the experimental data shows fit to both Freundlich and Langmuir isotherm models, with R^2 >0.92

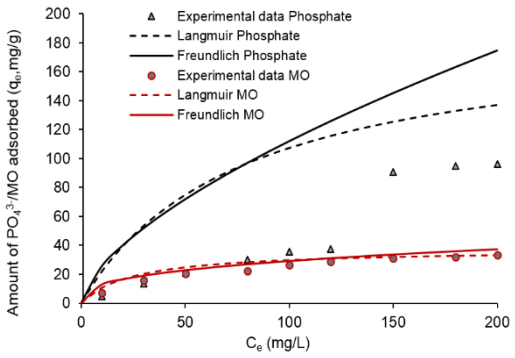

Fig. 7: Langmuir and Freundlich isotherms of PO_4^{3-}/MO adsorption on Fe_3O_4-biochar.

for PO_4^3 adsorption, and R^2 >0.96 for MO adsorption. These findings indicate that in the adsorption to phosphate and MO of Fe_3O_4-biochar with a single molecular layer and multi-molecular layer adsorption, numerous inequality and uniform surfaces are present in the Fe_3O_4-biochar surface, and adsorption may involve a variety of interactive relationships between the absorbent and the adsorbate [1]. The adsorption to phosphate of Ca-Mg-loaded biochars were also well fitted to the Freundlich (R^2 > 0.95) and Langmuir model (R^2 > 0.94) [1]. Using a magnetic biochar from sewage sludge with $SrFe_{12}O_{19}$ as magnetic substrate, the Langmuir model (R^2 > 0.98) better described the adsorption of MO than the Freundlich model (R^2 > 0.95) [42].

Under the optimum adsorption conditions, the maximum adsorption capacity of Fe_3O_4-biochar for PO_4^{3-} was 189.2 mg/g while that of MO was 37.31 mg/g (Table 2), The adsorption capacity of Fe_3O_4-biochar for PO_4^{3-} therefore, is close to 5 times greater than MO.

From the available literature, the reported adsorption mechanisms between PO_4^{3-} and Fe_3O_4-biochar was somewhat different from that found between MO and Fe_3O_4-biochar. The mechanisms of the PO_4^{3-} adsorption with Fe_3O_4-biochar might vary depending upon

Table 2: The Langmuir and Freundlich isotherm parameters for PO_4^{3-}/MO adsorption onto Fe_3O_4-biochar.

Isotherm models		PO_4^{3-}	MO
Langmuir	R^2	0.92	0.96
	q_m (mg/g)	189.2	37.31
	k_L (L/mg)	0.013	0.10
Freundlich	R^2	0.93	0.97
	k_F ((mg/kg)/(mg/L)^n)	5.83	5.65
	1/n	1.56	2.81

Fig. 8: Fe_3O_4-biochar collected PO_4^{3-} or MO from the suspension by a magnet.

electrostatic interactions, Lewis acid–base interaction, ion exchange, ligand exchange, precipitation, crystallization, inner sphere complexation, outer sphere complexation and hydrogen bonding [15]. Whereas, for MO dye, several mechanisms might be involved, including π-π interactions, hydrogen bond, electrostatic attraction and hydrophobic interaction [43]. Therefore, the physical and chemical forces governed the adsorption of PO_4^{3-} onto Fe_3O_4-biochar, while something more than forces governed the adsorption of MO onto Fe_3O_4-biochar, leading the higher in the maximum adsorption capacities for PO_4^{3-}, as is found in this work.

Fig. 8 demonstrates the ability to collect Fe_3O_4-biochar after being used for PO_4^{3-} and MO adsorption. Fe_3O_4-biochar can be re-collected *rapidly* from the suspension of adsobent and PO_4^{3-}-contaminated water or MO^--contaminated water, by an external magnet.

Comparison with other adsorbents

The adsorption capacity of Fe_3O_4-biochar derived from rice straw for PO_4^{3-} and MO has been compared with other magnetic biochar materials as presented in Table 3. For PO_4^{3-} adsorption, it shows that the Fe_3O_4-biochar from rice straw studied in this work has a comparative adsorption capacity to PO_4^{3-} compared to some other Fe-based biochar adsorbents. For MO adsorption, however, the adsorption capacity of MO is less than others.

CONCLUSIONS

In this study, Fe_3O_4-biochar were synthesized by the co-precipitation method and used to adsorb PO_4^{3-} and MO from aqueous solutions in batch adsorption experiments. . Several techniques and methodologies (SEM/EDX, FTIR, N_2 adsorption-desorption isotherms and pH_{pzc} measurements) demonstrated that the Fe_3O_4-biochar was successfully synthesized and deposited on the surface of the pristine biochar. Examination of the adsorption isotherms revealed that the adsorption of PO_4^{3-} and MO are well described by both the Langmuir and Freundlich models. The theoretical maximum adsorption capacities of Fe_3O_4-biochar toward PO_4^{3-} (189.2 mg/g) were comparatively higher than the capacities for MO (37.31 mg/g) at pH 2. The adsorption capacity of Fe_3O_4-biochar for PO_4^{3-} therefore is close to 5 times greater than MO. The pseudo-second-order kinetic model adequately described the kinetic data for both PO_4^{3-} and MO, and

Table 3: Comparison of PO43- and MO adsorption capacities of Fe3O4-biochar derived from rice straw with those of other Fe-based biochar adsorbents.

Adsorbate	Adsorbent	Magnetic methods	Adsorption capacity (mg/g)	Experimental conditions	Ref.
PO_4^{3-}	Fe-modified coconut shell biochar	impregnation-pyrolysis	36	pH of 7.0; 24h contact time, at 25°C	[35]
	Magnetic water hyacinth biochar	co-precipitation	5.07	pH of 7.0; 24h contact time, at 25°C	[44]
	Fe-impregnated woodchip biochar	impregnation	3.2	pH of 5.6; 24h contact time, at 24°C	[45]
	Fe^{3+}/Fe^{2+} modified waste activated sludge biochar	co-precipitation	34.2	pH of 7.0; 2h contact time, at 22°C	[46]
	Magnetic Fungi (*N.crassa*) biochar	impregnation	23.9	24h contact time, at 25°C	[47]
	Magnetic douglas fir biochar	co-precipitation	91.3	pH of 3.0; 2h contact time, at 25°C	[48]
	Fe_3O_4-biochar from rice straw	co-precipitation	189.2	pH of 2; 240min contact time; at 25°C	This study
MO	magnetic sewage sludge biochar	using $SrFe_{12}O_{19}$ as magnetic substrate	149.18	pH of 5.0; 40min contact time, at 25°C	[42]
	Fe_2O_3–biochar derived from pulp and paper sludge	impregnation	20.53	pH of 8; 30min contact time	[26]
	magnetic activated carbons	co-precipitation	84	pH of 2.78; 60min contact time; at 25°C	[49]
	Fe_3O_4-biochar from rice straw	co-precipitation	37.31	pH of 2; 240min contact time; at 25°C	This study

the equilibrium was achieved within 240 min. The obtained results suggested that Fe_3O_4-biochar from rice straw can be used as potential adsorbent to remove PO_4^{3-} and MO from aqueous media. Further research should include scaling up to a pilot study to better establish the efficacy of the Fe_3O_4-biochar adsorbent, assessing the different mass ratios of iron in biochar on the adsorptive process and removal mechanism of phosphate and methyl orange elimination from the water phase, evaluating the regeneration capacity of the Fe_3O_4-biochar adsorbens and the effect of competition on the adsorption of different anions.

Acknowledgements

The authors wish to thank Tran Hoang Kha, Kieu Thi Khanh, Pham Thi Ngoc Tran, Pham Thi Chuc Lan, Nguyen Hoang Son for their assistance with the experiment.

Received : Mar. 17, 2022 ; Accepted : Jun. 13, 2022

REFERENCES

[1] Yi M., Chen Y., Enhanced Phosphate Adsorption on Ca-Mg-Loaded Biochar Derived from Tobacco Stems, *Water Sci. Technol.*, **78(11)**: 2427-2436 (2018).

[2] White R.E., "Soils for fine wines", Oxford University Press (2003).

[3] Wilbers G. J., Becker M., Sebesvari Z., Renaud F. G., Spatial and temporal Variability of Surface Water Pollution in the Mekong Delta, Vietnam, *Sci. Total Environ.*, **485**: 653-665 (2014).

[4] Guo W., Ngo H.H., Surampalli R.Y., Zhang T.C., "Sustainable Resource Management: Technologies for Recovery and Reuse of Energy and Waste Materials", John Wiley & Sons (2021).

[5] Verma A.K., Dash R.R., Bhunia P., A Review on Chemical Coagulation/Flocculation Technologies for Removal of Colour from Textile Wastewaters, *J. Environ. Manage.*, **93(1)**: 154-68 (2012).

[6] Wu L., Liu X., Lv G., Zhu R., Tian L., Liu M., Li Y., Rao W., Liu T., Liao L., Study on the Adsorption Properties of Methyl Orange b Natural One-Dimensional Nano-Mineral Materials with Different Structures, *Sci. Rep.*, **11(1)**: 1-11 (2021).

[7] Oğuz E., Gürses A., Canpolat, N., Removal of Phosphate from Wastewaters, *Cem. Concr. Res.*, **33(8)**: 1109-1112 (2003).

[8] Gautam R. K., Banerjee S., Gautam P. K., Chattopadhyaya M. C., Remediation Technologies for Phosphate Removal from Wastewater: An Overview, in Daniels J.A. (Ed.) "Advances in Environmental Research", Nova Science Publishers, New York, pp 177-201 (2015).

[9] Lamari R., Benotmane, B., Mostefa, F., Removal of Methyl Orange from Aqueous Solution Using Zeolitic Imidazolate Framework-11: Adsorption Isotherms, Kinetics and Error Analysis, *Iran. J. Chem. Chem.Eng. (IJCCE)*, **41(6)**: 1985-1999 (2022).

[10] Abdelhafez A., Abbas M., "Applications of Biochar for Environmental Safety", BoD–Books on Demand (2020).

[11] Jiao G.J., Ma J., Li Y., Jin D., Guo Y., Zhou J., Sun R., Enhanced adsorption Activity for Phosphate Removal by Functional Lignin-Derived Carbon-Based Adsorbent: Optimization, Performance and Evaluation, *Sci. Total Environ.*, **761**: 143217 (2021).

[12] Abo Markeb A., Alonso A., Dorado A.D., Sánchez A., Font X., Phosphate removal and Recovery from Water Using Nanocomposite of Immobilized Magnetite Nanoparticles on Cationic Polymer, *Environ. Technol.*, **37(16)**: 2099-2112 (2016).

[13] Gustafsson J.P., Renman A., Renman G., Poll K., Phosphate Removal by Mineral-Based Sorbents Used in Filters for Small-Scale Wastewater Treatment, *Water Res.*, **42(1-2)**: 189-197 (2008).

[14] Bellier N., Chazarenc F., Comeau Y., Phosphorus Removal From Wastewater by Mineral Apatite, *Water Res.*, **40(15)**: 2965-2971 (2006).

[15] Almanassra I.W., Mckay G., Kochkodan V., Atieh M.A., Al-Ansari T., A state of the Art Review on Phosphate Removal from Water by Biochars, *Chem. Engin. J.*, 409:128211 (2021).

[16] Thanh V. Grain and Feed Update January 2020. USDA, Foreign Agricultural Service GAIN Report VM2020-0070. (2020).

[17] Mehmood I., Bari A., Aslam M.M., Okal E.J., Riaz M., ul Qamar M.T., Adnan M., Ahmed M., Saud S., Wahid F., Noor M., Fahad S., Biochar: An Adsorbent to Remediate Environmental Pollutants, in Fahad S., Sonmez O., Saud S. Wang D., Adnan M., Arif M. (Eds) "Engineering Tolerance in Crop Plants Against Abiotic Stress", CRC Press, pp 1-26 (2021).

[18] Chen B., Chen Z., Lv S., A Novel Magnetic Biochar Efficiently Sorbs Organic Pollutants and Phosphate, *Bio. Technol.*, **102(2)**: 716-723 (2011).

[19] Li X., Wang C., Zhang J., Liu J., Liu B., Chen G., Preparation and Application of Magnetic Biochar in Water Treatment: A Critical Review, *Sci. Total Environ.*, **711**: 134847 (2020).

[20] Zhao C., Wang B., Theng B.K., Wu P., Liu F., Wang S., et al., Formation and Mechanisms of Nano-Metal Oxide-Biochar Composites for Pollutant Removal: A Review, *Sci. Total Environ.*, 145305 (2021).

[21] Fang L., Li J-s, Donatello S., Cheeseman C., Poon C.S., Tsang D.C., Use of Mg/Ca Modified Biochars to Take Up Phosphorus from Acid-Extract of Incinerated Sewage Sludge Ash (ISSA) For Fertilizer Application, *J. Clean Pro.*, **244**: 118853 (2020).

[22] Zhang T., Wang Q., Deng Y., Jiang R., Recovery of Phosphorus from Swine Manure by Ultrasound/H2O2 Digestion, Struvite Crystallization, and Ferric Oxide Hydrate/Biochar Adsorption, *Front Chem.*, **6**: 464 (2018).

[23] Wang J., Chen W., Zhang M., Zhou R., Li J., Zhao W., et al., Optimize the Preparation of Fe_3O_4-Modified Magnetic Mesoporous Biochar and its Removal of Methyl Orange in Wastewater, *Environ. Monitor Assess.*, **193(4)**:1-20 (2021).

[24] Sun P., Hui C., Khan R.A., Du J., Zhang Q., Zhao Y.H., Efficient Removal of Crystal Violet Using Fe_3O_4-Coated Biochar: The Role of the Fe_3O_4 Nanoparticles and Modeling Study their Adsorption Behavior, *Sci. Rep.*, **5(1)**:1-12 (2015).

[25] Phuong D. T. M., Loc N.X., Miyanishi T., Efficiency of Dye Adsorption by Biochars Produced from Residues of Two Rice Varieties, Japanese Koshihikari and Vietnamese IR50404, *Desalin. Water Treat.*, **165**: 333-351 (2019).

[26] Chaukura N., Murimba E. C., Gwenzi W., Synthesis, Characterisation and Methyl Orange Adsorption Capacity of Ferric Oxide–Biochar Nano-Composites Derived from Pulp and Paper Sludge, *Appl. Water Sci.*, **7(5)**: 2175-2186 (2017).

[27] Zubair M., Manzar M. S., Suleiman M.A., Fernandes D.P., Meili L., Ayman W., ... & Haladu S.A., Enhanced Adsorption of Phosphate onto Magnetic Biochar-Steel Dust Composites from Waste, *Performance and Mechanism* (2022).

[28] Qin X., Luo J., Liu Z., Fu Y., Preparation and Characterization of MgO-Modified Rice Straw Biochars, *Molecules*, **25(23)**: 5730 (2020).

[29] Kumar R., "Surface Characterization Techniques: from Theory to Research", Walter de Gruyter GmbH & Co KG (2022).

[30] Sing K. S., Reporting Physisorption Data for Gas/Solid Systems With Special Reference to the Determination of Surface Area and Porosity (Recommendations 1984), *Pure Appl. Chem.*, **57(4)**: 603-619 (1985).

[31] Khalith, S. M., Ramalingam, R., Karuppannan, S. K., Dowlath, M. J. H., Kumar, R., Vijayalakshmi, S., Maheshwari, R. U., Arunachalam, K. D., Synthesis and Characterization of Polyphenols Functionalized Graphitic Hematite Nanocomposite Adsorbent from an Agro Waste and its Application for Removal of Cs from Aqueous Solution, *Chemosphere*, **286**: 131493 (2022).

[32] Santhosh C., Daneshvar E., Tripathi K.M., Baltrėnas P., Kim T., Baltrėnaitė E., et al., Synthesis and Characterization of Magnetic Biochar Adsorbents for the Removal of Cr (VI) and Acid Orange 7 dye from Aqueous Solution, *Environ. Sci. Pol. Res.*, **27(26)**: 32874-32887 (2020).

[33] Omran, M., & Fabritius, T., Effect of Steelmaking Dust Characteristics on Suitable Recycling Process Determining: Ferrochrome Converter (CRC) and Electric Arc Furnace (EAF) Dusts, *Powder Technol.*, 308: 47-60 (2017).

[34] Devi P., Saroha A.K., Utilization of Sludge Based Adsorbents for the Removal of Various Pollutants: A Review, *Sci. Total Environ.*, **578**: 16-33 (2017).

[35] Zhong Z., Yu G., Mo W., Zhang C., Huang H., Li S., Gao M., Lu X., Zhang B., Zhu, H., Enhanced Phosphate Sequestration by Fe (Iii) Modified Biochar Derived from Coconut Shell, *RSC Adv.*, **9(18)**: 10425-10436 (2019).

[36] Zeng L., Li X., Liu J., Adsorptive Removal of Phosphate from Aqueous Solutions Using Iron Oxide Tailings, *Water Res.*, **38(5)**: 1318-1326. (2004).

[37] Yu G., Zhang B., Lu X., Li J., Chen J., Zuo J., Efficient Removal of Phosphorus in Bioretention System by Sludge Pyrolysis Residue, *Arab. J. Geosci.*, **8(6)**: 3491-3499 (2015).

[38] Akama E., Tong A. J., Ito M., Tanaka S., The Study of the Partitioning Mechanism of Methyl Orange in an Aqueous Two-Phase System, *Talanta*, **48**: 1133–1137 (1999).

[39] Ma J., Yu F., Zhou L., Jin L., Yang M., Luan J., Tang Y., Fan H., Yuan Z., Chen J., Enhanced Adsorptive Removal of Methyl Orange and Methylene Blue from Aqueous Solution by Alkali-Activated Multiwalled Carbon Nanotubes, *App.l Mater. Interfaces*, **4**: 5749–5760 (2012).

[40] Cheng H., Liu Y., Li X., Adsorption Performance And Mechanism of Iron-Loaded Biochar to Methyl Orange in the Presence of Cr^{6+} from Dye Wastewater, *J. Hazar. Mater.*, **415**: 125749 (2021).

[41] Phuong D.T.M., Loc N.X., Rice Straw Biochar and Magnetic Rice Straw Biochar for Safranin O Adsorption from Aqueous Solution, *Water*, **14(2)**: 186. (2022).

[42] Zhang J., Liu M., Yang T., Yang K., Wang H., Synthesis and Characterization of a Novel Magnetic Biochar from Sewage Sludge and its Effectiveness in the Removal of Methyl Orange from Aqueous Solution, *Water Sci. Technol.*, **75(7)**: 1539-1547 (2017).

[43] Tan X-f, Liu Y-g, Gu Y-l, Xu Y, Zeng G-m, Hu X-j, Liu S-b, Wang X., Liu S-m, Li J., Biochar-Based Nano-Composites for the Decontamination of Wastewater: A Review, *Biores. Technol.*, **212**: 318-333 (2016).

[44] Cai R., Wang X., Ji X., Peng B., Tan C., Huang X., Phosphate Reclaim from Simulated and Real Eutrophic Water by Magnetic Biochar Derived from Water Hyacinth, *J. Environ. Manage.*, **187**: 212-219 (2017).

[45] Micháleková-Richveisová B., Frišták V., Pipíška M., Ďuriška L., Moreno-Jimenez E., Soja G., Iron-Impregnated Biochars as Effective Phosphate Sorption Materials, *Environ. Sci. Pol. Res.*, **24(1)**: 463-475 (2017).

[46] Yang Q., Wang X., Luo W., Sun J., Xu Q., Chen F., et al., Effectiveness and Mechanisms of Phosphate Adsorption on Iron-Modified Biochars Derived from Waste Activated Sludge, *Biores. Technol.*, **247**: 537-44 (2018).

[47] Jack J., Huggins T.M., Huang Y., Fang Y., Ren Z.J., Production of Magnetic Biochar From Waste-Derived Fungal Biomass for Phosphorus Removal and Recovery, *J. Clean Pro.*, **224**:100-106 (2019).

[48] Karunanayake A.G., Navarathna C.M., Gunatilake S.R., Crowley M., Anderson R., Mohan D., et al., Fe_3O_4 Nanoparticles Dispersed on Douglas Fir Biochar for Phosphate Sorption, *ACS Appl. Nano Mater.*, **2(6)**: 3467-3479 (2019).

[49] Cordova Estrada A.K., Cordova Lozano F., Lara Díaz R.A., Thermodynamics and Kinetic Studies for the Adsorption Process of Methyl Orange by Magnetic Activated Carbons, *Air Soil Water Res.*, **14**: 1-11 (2021).